Numerical modeling of two-photon focal modulation microscopy with a sinusoidal phase filter

Rui Chen
Shuhao Shen
Nanguang Chen

SPIE.

Numerical modeling of two-photon focal modulation microscopy with a sinusoidal phase filter

Rui Chen, Shuhao Shen, and Nanguang Chen*
National University of Singapore, Department of Biomedical Engineering, Singapore

Abstract. A spatiotemporal phase modulator (STPM) is theoretically investigated using the vectorial diffraction theory. The STPM is equivalent to a time-dependent phase-only pupil filter that alternates between a homogeneous filter and a stripe-shaped filter with a sinusoidal phase distribution. It is found that two-photon focal modulation microscopy (TPFMM) using this STPM can significantly suppress the background contribution from out-of-focus ballistic excitation and achieve almost the same resolution as two-photon microscopy. The modulation depth is also evaluated and a compromise exists between the signal-to-background ratio and signal-to-noise ratio. The theoretical investigations provide important insights into future implementations of TPFMM and its potential to further extend the penetration depth of nonlinear microscopy in imaging multiple-scattering biological tissues. © *2018 Society of Photo-Optical Instrumentation Engineers (SPIE)* [DOI: 10.1117/1.JBO.23.5.055002]

Keywords: imaging through turbid media; nonlinear microscopy; diffraction theory; modulation techniques; phase-only filters.

Paper 170777RR received Nov. 30, 2017; accepted for publication Apr. 19, 2018; published online May 8, 2018.

1 Introduction

Being noninvasive and capable of subcellular resolution, optical microscopy has become a widely used tool in both biological research and clinical diagnostics to investigate biological tissues. Due to the strong scattering nature of biological tissues, penetration depth is a severe limitation for optical microscopy. Considerable efforts have been made to enhance the penetration depth of optical microscopy within scattering biological tissues.[1] With a detection pinhole to select ballistic photons from the focal plane and thus the optical sectional capability, confocal fluorescence microscopy can achieve diffraction-limited resolution with up to a few tens of micrometer depth only.[2] This is because the fine details of samples are easily masked by the background signal due to the strong scattering by various tissue components.[1] Another widely used deep-tissue optical imaging technique is optical coherence tomography (OCT).[1,3] OCT can achieve deeper penetration than confocal fluorescence microscopy; however, it is not compatible with fluorescence and also has two major disadvantages: (1) it has a lower resolution than the confocal microscopy and (2) the contrast is based on discontinuities in the real part of the indices of refractive at interfaces. Thus, it does not give molecular information.[4] In contrast to OCT, the development of two-photon microscopy (TPM) has significantly extended the penetration depth of molecular imaging for *in vivo* applications,[5,6] mainly by reducing the out-of-focus fluorescence excitation. The penetration depth can be further enhanced by reducing the pulse duty cycle or using longer wavelengths. For example, an imaging depth of 1 mm in mouse brains has been demonstrated by using a regenerative amplifier as the excitation light source.[7] On the other hand, using an excitation wavelength of 1280 nm, TPM enables deeper penetration up to 1 mm in *in vivo* imaging of mouse brains mainly due to the reduced tissue scattering at the longer wavelength.[8] However, only fluorescent probes at far-red wavelength can be employed

in this case. It should be noted that the excitation intensity in the focal region decreases exponentially with the increasing penetration depth and can be maintained by raising the excitation power at the surface of the biological tissue sample. However, this results in the enhancement of the background fluorescence signal and thus the imaging depth of TPM is fundamentally limited by the onset of out-of-focus fluorescence generation near the top of the sample.[9] Therefore, the focal plane signal could be easily overwhelmed by the out-of-focus signal at larger focal depths. Several techniques have been proposed to suppress out-of-focus contributions.[10–14] Differential aberration imaging (DAI) employs a deformable mirror to introduce illumination aberrations that preferentially degrade two-photon (TP) signal but leaving TP background relatively unchanged and then a simple subtraction of aberrated from unaberrated images results in background rejection.[10,11] By spatially separating spectral components of pulses into a "rainbow beam" and recombining these components only at the spatial focus of the objective lens, the technique of simultaneous spatial and temporal focusing of femtosecond pulses has been demonstrated to improve the signal-to-background ratio (SBR) in TPM.[12] Similar to the confocal fluorescent microscopy, a confocal pinhole has been employed to reject the out-of-focus signal in TPM, which could improve the penetration depth from 5 to 6.2 scattering mean free paths (SMFP) with a significant reduction of collection efficiency.[13] By modulating the spatial overlaps between two-color pulses, Isobe et al.[14] demonstrated background-free three-dimensional imaging in mouse brain tissues, which achieved out-of-focus signal suppression by a factor of 100 and lateral resolution enhancement by a factor of 1.6.

Recently, focal modulation microscopy (FMM) with single-photon (SP) fluorescence was developed to reject out-of-focus signal by bringing a spatiotemporal phase modulator (STPM) in a confocal laser scanning microscope, which had demonstrated

---

experimentally an imaging depth up to 600 μm in chicken cartilages.[15] The STPM is basically a time-dependent phase-only pupil filter, which repeatedly switches between a homogeneous filter and an inhomogeneous filter. When the STPM is homogeneous, the excitation beam is properly focused into the focal volume by the following objective lens. The inhomogeneous filter is so designed that it leads to redistribution of the excitation beam and minimize the focal intensity. Consequently, the STPM generates a periodic intensity modulation that is essentially confined to the focal volume. Fluorescence emissions from the focal volume are also modulated at the same frequency while the background related to scattered excitation light is essentially constant and can be effectively removed using an appropriate demodulation scheme either in the time domain[1] or the spatial domain.[16,17]

One of the key STPM design issues is the spatial phase pattern of the inhomogeneous filter, which determines several FMM specifications such as modulation depth and background rejection. A few versions of STPM have been reported and it has been found that only ballistic excitation photons contribute to the modulated excitation intensity as these photons have well-defined phase and polarization; meanwhile, the contribution of scattered excitation is filtered out due to the demodulation mechanism used in FMM.[18,19] In these versions of the STPM, the inhomogeneous filter is typically chosen as a binary filter (phase values of 0 and π). Two-photon FMM (TPFMM) based on binary inhomogeneous filters is previously investigated using a theoretical model that combines the scalar diffraction theory and a Monte Carlo algorithm for tracking scattered light in turbid media.[20] However, this model is based on the paraxial approximation, and thus it may not be accurate for high numerical aperture (NA) cases. Some important parameters, such as the modulation depth and resolution, have not been investigated. More importantly, the binary filters used in this study have sharp phase transitions between zones that lead to intensity oscillations in the out-of-focus regions and therefore background modulation. Such a background modulation is enhanced by the quadratic dependence of the excitation rate on the excitation intensity. In a typical nondescanned TPM, no confocal pinhole is in place for background rejection. As a result, there is strong need to further improve our theoretical model and search for optimal filter designs for TPFMM.

In this paper, we propose an STPM design for TPFMM and validate its performance using numerical simulations based on the vectorial diffraction theory. It is noted that the scattered excitation is largely filtered out in FMM due to the demodulation scheme.[18–20] Therefore, in this paper, only the ballistic excitation is considered in numerical simulations. The contribution of the paper is summarized as follows. First, while the most frequently used theoretical model of TPM is based on the paraxial approximation,[10,11,20] this paper employs the vectorial diffraction theory in the numerical simulations of TPFMM, which provides a more accurate model than the paraxial approximation when a high NA objective is present. Second, based on the vectorial model, a suitable STPM design that incorporates an inhomogeneous phase filter with sinusoidal distributions is presented and validated for TPFMM. Compared to binary phase filters, sinusoidal phase filters can significantly mitigate the oscillation of intensity distribution near the transition regions (binary phase sharp transition) and, thus, is beneficial to the background rejection in the turbid media. We also evaluate the spatial resolution, modulation depth, and signal-to-background ratio, which are related to the inhomogeneous stripe-shaped filter with a sinusoidal phase distribution. It is found that TPFMM with the proposed STPM can achieve almost the same resolution as TPM with improved background suppression. Such investigations provide valuable guidance for the future implementations and experiments for deep-tissue imaging.

2 Vectorial Model of the TPFMM

This section provides a quantitative description of the vectorial model of the TPFMM, which is formulated by the vectorial diffraction theory. We consider an ideal sample where the fluorophore concentration is uniformly distributed throughout the sample. To simplify the derivation, we also assume that the excitation wavelength λ is exactly twice as large as the emitted TP fluorescence wavelength, i.e., the Stoke's shift is neglected. The basic TPFMM is the same as the conventional TPM except for the STPM design in the illumination path and demodulation circuits in the signal detection. Using the appropriate demodulation scheme, the background related to the scattered excitation light, which is essentially constant, can be effectively removed.[1,20] In the following treatment, we have assumed that TPM background is generated exclusively by out-of-focus ballistic excitation. The schematic diagram of FMM with the phase filter is shown in Fig. 1(a). According to the Richards–Wolf integral,[21] the electric field at (x, y, z) in the Cartesian coordinates system is determined as

$$\mathbf{E}(x, y, z) = -\frac{ik_{\text{obj}}f_{\text{obj}}e^{ik_{\text{obj}}f_{\text{obj}}}}{2\pi} \int_0^{\theta_{\max}} \int_0^{2\pi} \overline{\overline{\mathbf{T}}} \cdot \mathbf{E}_0(\theta, \phi) a(\theta, z) e^{ig(\theta,\phi)} \cos^{1/2}\theta e^{ik_{\text{obj}}[\rho \sin\theta \cos(\phi-\varphi)-z\cos\theta]} \sin\theta d\theta \, d\phi, \tag{1}$$

where $\rho = \sqrt{x^2 + y^2}$ and $\varphi = \tan^{-1}(y/x)$. Here, $\overline{\overline{\mathbf{T}}}$ is the transformation dyadic matrix, which can be expressed as[22]

$$\overline{\overline{\mathbf{T}}} = \begin{bmatrix} (1 + \cos\theta) - (1 - \cos\theta)\cos 2\phi & -(1 - \cos\theta)\sin 2\phi & -2\sin\theta\cos\phi \\ -(1 - \cos\theta)\sin 2\phi & (1 + \cos\theta) + (1 - \cos\theta)\cos 2\phi & -2\sin\theta\cos\phi \\ 2\sin\theta\cos\phi & 2\sin\theta\sin\phi & 2\cos\theta \end{bmatrix}, \tag{2}$$

where $g(\theta, \phi)$ denotes the pupil filter function that describes the phase distribution at the lens aperture. $\theta_{\max}$ is the angular semi-aperture and the NA of the objective lens is determined by the product of the refractive index of the object space n_{obj} and

$\sin\theta_{\max}$. The wavenumber k_{obj} is given by $k_{\text{obj}} = 2\pi n_{\text{obj}}/\lambda$ and f_{obj} is the focal length of the objective lens. $\mathbf{E}_0(\theta, \phi) = \hat{x} \exp(-\frac{\sin^2\theta}{\sin^2\theta_{\max}})$ defines a Gaussian beam with x-direction linear polarization. It is known that the strong attenuation is expected

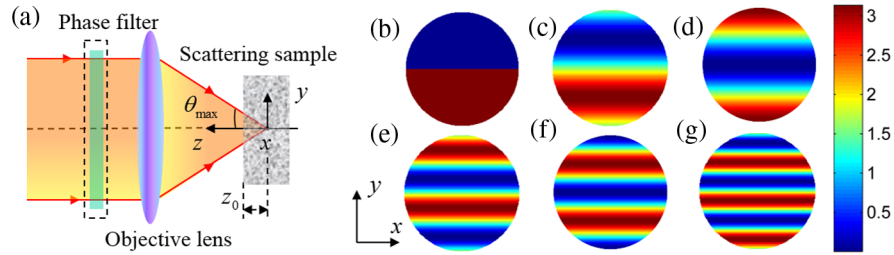**Fig. 1** Inhomogeneous phase filters for FMM. The minimum and maximum phases are 0 and π. (a) The schematic diagram of FMM with the phase filter. z_0 is the imaging depth in the scattering sample. (b) Two-zone stripe-shaped filter with a binary phase distribution, which is the filter used in the first prototype of SPFMM.[15] (c)–(g) Two to six zones stripe-shaped filters with sinusoidal phase distributions. The phase distribution of the filters is defined by Eq. (6).

in high NA imaging for the absorbing-scattering tissue sample.[7] The z-dependent angular attenuation term $a(\theta, z)$ is defined as

$$a(\theta, z) = \begin{cases} \exp\left(-\frac{\alpha}{2}\frac{z_0 - z}{\cos\theta}\right) & z \leq z_0 \\ 1 & z > z_0 \end{cases}, \quad (3)$$

where z_0 is the imaging depth as shown in Fig. 1(a). $\alpha = 1/l_s$ is the scattering coefficient and l_s is the SMFP. The excitation light intensity is simply given as

$$I(x, y, z) = |\mathbf{E}(x, y, z)|^2. \quad (4)$$

As the molecular excitation rate is proportional to the squared excitation intensity in a TPM,[2,23] the excitation rate of TPM is given by $I^2(x, y, z)$. According to the principle of the FMM,[1,15] the effective excitation rate of TPFMM is defined as

$$I_{\text{EX}}(x, y, z) = I^2_{\text{max}} - I^2_{\text{min}}, \quad (5)$$

where I^2_{max} and I^2_{min} are the TP excitation rates with a homogeneous phase filter $g_{\text{max}}(\theta, \phi) = 0$ and an inhomogeneous phase filter $g_{\text{min}}(\theta, \phi)$, respectively. $I_{\text{EX}}(x, y, z)$ can also be considered as the point spread function (PSF) of the TPFMM. Mathematically, the effective excitation rate of TPFMM is a subtraction of a TPM image using an inhomogeneous phase filter from another image using a homogeneous phase filter. In the DAI,[10,11] the result is a simple subtraction of aberrated from unaberrated images as well. However, modulation and demodulation in TPFMM are performed in the timescale of microsecond. Consequently, TPFMM is more immune to imaging artifacts arising from fluorophore photobleaching, blinking, sample motion, laser power fluctuation, detector gain fluctuation, and environment light interference.

Usually, a femtosecond laser, such as a Ti:sapphire laser, is used for multiphoton excitation. In the following simulations, we assume that the center wavelength of the laser light is 800 nm and the spectral width of 20 nm is sampled at 101 discrete wavelengths. As an example, a water immersion objective lens with NA = 1.0 and $n_{\text{obj}} = 1.33$ is used for the following simulation.

3 Advantage of Sinusoidal Phase Filters in TPFMM

In FMM, one of the key STPM design issues is the spatial phase pattern of the inhomogeneous filter $[g_{\text{min}}(\theta, \phi)]$. Compared to the annular filters, stripe-shaped filters are easier to be fabricated and less sensitive to alignment drifts. In the single-photon focal

modulation microscopy (SPFMM), stripe-shaped filters with binary phases (0 and π) are used. In this section, we propose the stripe-shaped filter with the sinusoidal phase distribution and show that it is superior to the stripe-shaped filter with the binary phase distribution for TPFMM. The phase distribution of the stripe-shaped filter is defined as

$$g_{\text{min}}(\theta, \phi) = \begin{cases} \frac{\pi}{2} - \frac{\pi}{2}\cos\left(\frac{N-1}{2}\pi\frac{\sin\theta\sin\phi}{\sin\theta_{\text{max}}}\right) & N: \text{odd integer} \\ \frac{\pi}{2} - \frac{\pi}{2}\sin\left(\frac{N}{2}\pi\frac{\sin\theta\sin\phi}{\sin\theta_{\text{max}}}\right) & N: \text{even integer} \end{cases}, \quad (6)$$

where N is the number of the zone in the phase filter.

The two-zone stripe-shaped filters with binary phase and sinusoidal phase distribution are shown in Figs. 1(b) and 1(c), respectively. The effective excitation rates in out-of-focus planes are simulated to estimate their contributions and effects to the fluorescence background. As an example, Fig. 2 shows excitation rate distributions at a plane of 500 μm defocus for SPFMM and TPFMM with the two-zone filters, respectively, when a water immersion objective with NA = 1.0 and $n_{\text{obj}} = 1.33$ is used. For both SPFMM and TPFMM, it is expected that the background contribution using the two-zone sinusoidal phase filter in the phase transition region is much lower than that using the two-zone binary phase filter. In order to show the details, the cross section along the y axis is also shown in Fig. 3. It is found that the excitation rate on axis for both filters is much higher than that of the surrounding region, as shown in Figs. 3(a) and 3(b), which can be recognized as interference effect between the incident beams.[24] The on-axis intensity for the sinusoidal filter is also present in the zoom-in insets of Figs. 2(d) and 2(h).

Due to the wave property of light, there are fast spatial oscillations in the excitation light even when the pupil filter is homogeneous,[25] as one can see in the red curves in Fig. 3. In case of inhomogeneous filters, much stronger oscillations are observed especially in regions corresponding to rapid phase changes. It is apparent, however, that the sinusoidal phase filter leads to much weaker oscillations (blue curves) than the binary filter (black curves). More specifically, compared with the two-zone binary phase filter, the two-zone sinusoidal phase filter can significantly mitigate the oscillation of intensity distribution near the transition region with some minor ripples generated away from the phase transition region.

For SPFMM, the out-of-focus excitation light oscillation is not a big problem due to two reasons. First of all, a confocal pinhole is employed to significantly suppress its contribution. Second, the integration of the oscillatory component over the
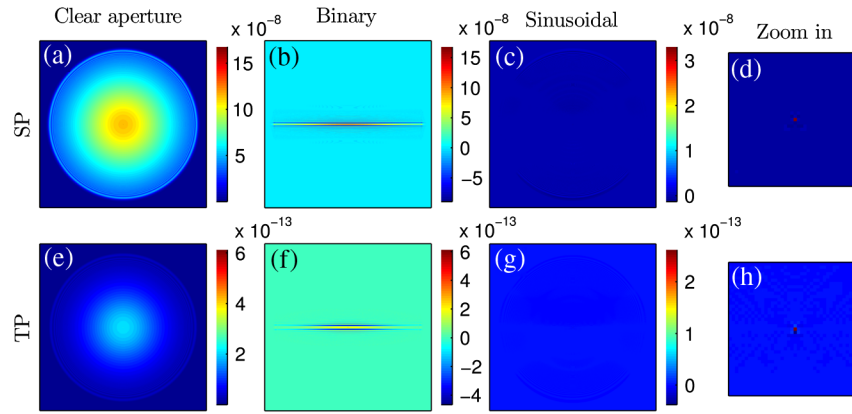
Fig. 2 Normalized excitation rate distributions of (a–c) SPFMM and (e–g) TPFMM at a defocus plane (500 μm) using two-zone filters when the water immersion objective lens with NA = 1.0 and n_{obj} = 1.33 is used. SP and TP cases are provided in the first column (clear aperture) for comparison. The second and the third columns are the FMM with binary and sinusoidal phase distributions, respectively. (d) and (h) are two zoom-in figures from the center part of (c) and (g), respectively. All these data are normalized by the peak excitation rate of SP and TP cases in the focal plane, respectively. The horizontal and vertical dimensions of (a–c, e–g) are [−625, 625] μm for both x axis and y axis while the dimensions of (d, h) are 50 μm × 50 μm.

defocus plane is simply zero. However, the situation in nonlinear optical microscopy is very different and is worthy of thorough investigation. The quadratic dependence of the excitation rate on the excitation light intensity in TPM enhances the spatial oscillation and skews the spatial average to a negative value. In addition, nondescanned detection is usually employed in TPM. In this case, there is no confocal pinhole to reject the out-of-focus fluorescence. Therefore, the binary phase filters designed for previously reported SPFMM may not be an ideal choice for TPFMM. Compared with the binary phase filter, the sinusoidal phase filter is a good candidate for TPFMM since the sinusoidal phase filter can significantly mitigate the oscillation of the

intensity distribution near the transition region as shown in Fig. 3(b). We also evaluate more sinusoidal phase filters with different numbers of zones [Figs. 1(d)–1(g)] in an attempt to figure out an optimal design, which shows the similar effect with the two-zone filter.

4 TPFMM with Stripe-Shaped Sinusoidal Filters

In this section, the performance of TPFMM with stripe-shaped sinusoidal filters is evaluated and several characteristics, including PSF, modulation depth, resolution, background suppression as well as signal-to-background ratio, are investigated for various sinusoidal filters.

4.1 Point Spread Function of TPFMM with Stripe-Shaped Filters

For FMM, the intensity modulation is essentially confined within the focal volume by modulating the phase distribution of the illumination beam. The PSF of TPFMM can be computed using Eq. (5) with the attenuation term removed. The PSF cross sections along three axes are shown in Fig. 4 where the water immersion objective lens with NA = 1.0 is employed. The stripe-shaped phase filters in Figs. 1(b)–1(g) are included in the simulation. It is shown that the focal volume of TPFMM for all the stripe-shaped phase filters is almost same as that of TPM except that negative sidelobes appear in the y axis and z axis as shown in Figs. 4(b) and 4(c). It is also found that the PSF intensity distributions along the x axis for all the phase filters coincide due to the phase variation along the y-axis only. For intensity distribution along the y axis, the sinusoidal phase filters with even number zones show asymmetrical intensity distributions while those with odd number zones show symmetrical intensity distributions. This is because the symmetry of phase distribution of the filters with even number and odd number zones is different, one is central symmetry and the other one is axial symmetry as shown in Figs. 1(c)–1(g). On the other hand, with the increase of the zone number, negative sidelobes shift away from the central peak of the PSF and their magnitudes
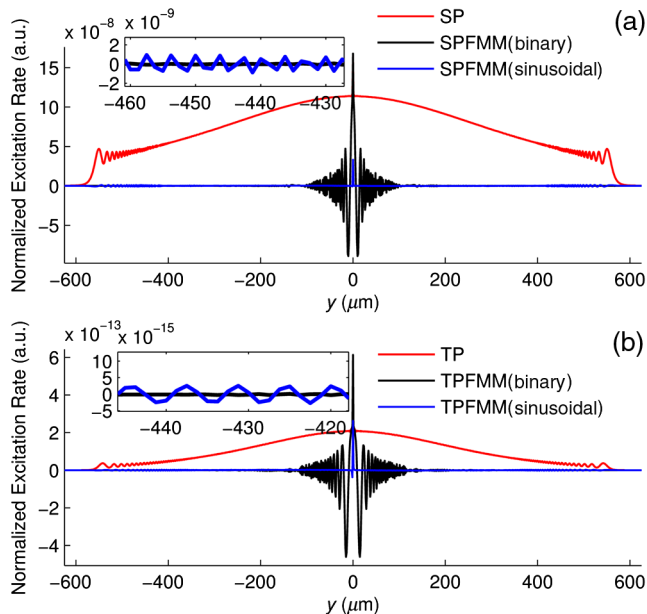

Fig. 3 Normalized excitation rate distributions of (a) SPFMM and (b) TPFMM along the y axis at defocus plane 500 μm using two-zone binary and sinusoidal phase filters, respectively, when the water immersion objective lens with NA = 1.0 and n_{obj} = 1.33 is used. The zoom-in insets show the details of the normalized excitation rate.
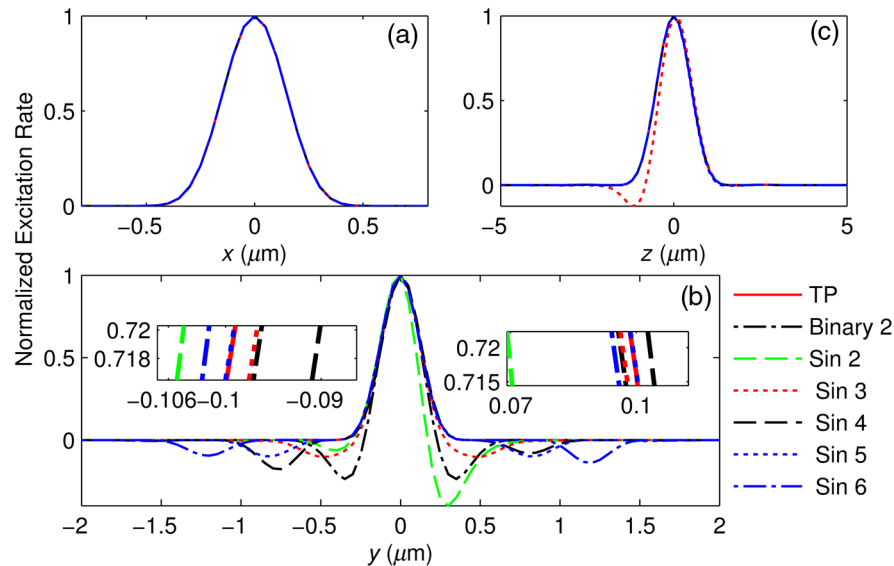
Fig. 4 The normalized PSF of TPFMM using binary and sinusoidal phase filters in Fig. 1, when the water immersion objective lens is used. (a) x axis, (b) y axis, and (c) z axis. For comparison, the PSF of TP is also provided. In (a), the PSFs for various phase filters along the x axis coincide with that of the TP case. This is because stripe-shaped phase filters vary along the y axis. Two zoom-in insets are included in (b).

are reduced. For intensity distribution along the z axis, in fact, the PSF with even number zones phase filter is symmetrical and the PSF with odd number zones is not symmetrical, which is opposite to the PSF along the y axis. However, the difference except for three-zone case is so small that it has less effect on the resolution of TPFMM.

4.2 Resolution and Modulation Depth of TPFMM

The resolution of the TPFMM is defined as the full-width half-maximum (FWHM) of the normalized excitation rate distributions along the radial direction and axial direction. Due to the anisotropy between the x axis and y axis, we define $\mathrm{FWHM}_{xy} = \sqrt{\mathrm{FWHM}_x \times \mathrm{FWHM}_y}$ as the lateral resolution. The lateral and longitudinal resolution of TPFMM using various phase filters are shown in Table 1 for water immersion objective lenses. As references, the lateral and longitudinal resolution of TPM are 312 and 1140 nm for the water immersion objective lens. It is found that the lateral and longitudinal resolution of TPFMM are almost same as that of TPM, which means that TPFMM can achieve almost same resolution as TPM with the significant background rejection.

Another key parameter of FMM is the modulation depth since it determines the efficiency of the FMM signal generation and signal-to-noise ratio. The modulation depth is defined as the ratio of the intensity of the modulated fluorescence signal (i.e., the AC component) to the average intensity (the DC component) collected by the detector.[1] Computed modulation depths for the investigated filters are also shown in Table 1. With the number of zones increasing from two to eight, the modulation depth of both types increases from around 0.2 to around 0.5. This is because there are negative sidelobes in the effective PSF [Fig. 4(b)] of TPFMM as TPFMM is based on a differential excitation mechanism. As shown in Fig. 4(b), with an increase of the number of zones, sidelobes are shifted away from the central peak of PSF and their magnitude is reduced. Further, sidelobes for a binary phase transition filter are smaller than that for a sinusoidal phase filter. As a result, TPFMM with the former has a larger modulation depth than that with the latter. In practical situations for imaging biological specimens, the larger modulation depth enables a stronger FMM signal at the same level of the excitation loading. The typical modulation depths 0.3 to 0.8 can be found in Refs. 15, 17, and 19.

Table 1 Resolution and modulation depth of TPFMM with various phase filters (resolution unit: μm, NA = 1.0).

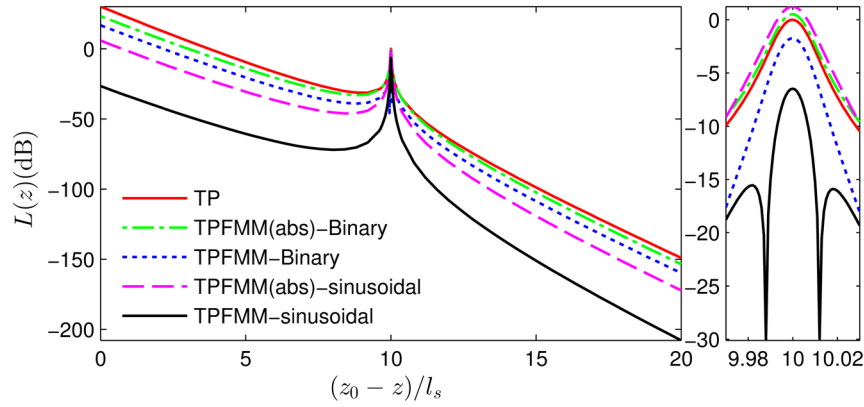| Zone number		2	3	4	5	6	7	8
Lateral	Binary	0.304	0.312	0.311	0.312	0.312	0.312	0.312
	Sinusoidal	0.292	0.308	0.309	0.312	0.311	0.312	0.312
Longitudinal	Binary	1.140	1.134	1.140	1.140	1.140	1.140	1.140
	Sinusoidal	1.146	1.041	1.141	1.134	1.140	1.139	1.140
Modulation depth	Binary	0.22	0.33	0.40	0.41	0.47	0.45	0.51
	Sinusoidal	0.14	0.20	0.33	0.35	0.41	0.42	0.45

Fig. 5 The comparison of the logarithmic integrated intensity $L(z)$ for two-zone binary and sinusoidal phase filters with the imaging depth $z_0 = 1$ mm and $l_s = 100$ μm. The inset on the right is the zoom-in figure near the focal plane of the sample. A water immersion objective with NA = 1.0 and $n_{obj} = 1.33$ is used.

4.3 Background Suppression

In the deep-tissue imaging, background suppression is very important. In Sec. 3, the excitation rate distributions at a defocus plane of TPFMM with the sinusoidal filters have been investigated. To quantify the background suppression capability and improvement, we have defined three system parameters. The first is the integrated intensity for depth z

$$I_{int}(z) = \int_{-\infty}^{+\infty} \int_{-\infty}^{+\infty} I_{EX}(x, y, z) dx\, dy, \tag{7}$$

where $I_{EX}(x, y, z)$ is the excitation rate. The integrated intensity is proportional to the fluorescence generated on the plane z in a homogeneous sample. In practice, however, the biological tissue sample is normally heterogeneous and this parameter may not be adequate. To take into account the worst scenario, we define an absolute integrated intensity as

$$I'_{int}(z) = \int_{-\infty}^{+\infty} \int_{-\infty}^{+\infty} |I_{EX}(x, y, z)| dx\, dy. \tag{8}$$

The third parameter is defined as a logarithmic integrated intensity ratio

$$L(z) = 10 \log_{10} |I_{int}(z)/I_{int\_TPM}(0)|, \tag{9}$$

which normalizes the integrated intensity or absolute integrated intensity at any depth z by that of the focal plane of TPM. Figure 5 shows the logarithmic integrated intensity ratios for TPM and TPFMM imaging with two-zone filters at a depth of 1 mm ($z_0 = 1$ mm), when a water immersion objective lens with NA = 1.0 is used. For TPM and TPFMM, if we increase the excitation power to maintain adequate ballistic power at the focal region, the out-of-focus background fluorescence can lead to significant power densities near the surface of the sample, which has been demonstrated by many researchers.[7,8,10] Compared to TPM, it is evident that TPFMM can largely reduce the contribution from out-of-focus ballistic excitation although the integrated intensity at the focal plane is slightly lower than that of TPM case, which is reflected in the inset of Fig. 5. Specifically, for the two-zone sinusoidal phase filter, the out-of-focus ballistic excitation in TPFMM is about 50 dB lower than

that in TPM at the defocus plane from 2 to 8 SMFP l_s and the near-surface out-of-focus ballistic excitation is about 56 dB lower than that in TPM. Even in the worst case [Eq. (8)], the background rejection improved by roughly 25 dB. However, for the binary phase filter in TPFMM, the best we can achieve is merely a 13-dB improvement. Therefore, compared to the two-zone binary filter, the two-zone stripe-shaped sinusoidal filter is a good candidate for TPFMM to achieve background suppression. As another example, Fig. 6 shows the logarithmic integrated intensity ratio using two-zone and six-zone sinusoidal filters for water immersion objective. For TPFMM with a six-zone sinusoidal phase filter, the out-of-focus ballistic excitation is about 36 dB lower than TPM with integrated intensity about 1.3 dB lower at the focal plane.

Figure 7 shows the improved surface background rejection, quantified by $L_{TPM}(z_0) - L_{TPFMM}(z_0)$, and the focal plane excitation intensities, quantified by $I_{int,TPFMM}(0)/I_{int,TPM}(0)$, for filters of various numbers of zones. As seen from Fig. 7(a), it is again verified that TPFMM with a sinusoidal phase filter always provides stronger background suppression than that with a sharp phase transition filter of the same number of zones. With an increasing number of zones, the background suppression capability of TPFMM is slightly decreased. This is because the more zones of the filters, the more oscillations of the effective excitation rate at out-of-focus planes. The integration of such oscillation leads to the higher background contribution.

However, for the definition in Eq. (7), the difference of near-surface out-of-focus ballistic excitation between TPM and TPFMM is oscillating. In order to explain this phenomenon, the effective excitation rates at out-of-focus planes (similar to Fig. 2) are simulated for different zone number filters. The presence of negative intensity and the different intensity distribution for odd and even number filters result in the oscillating phenomena of the background suppression curve.

Further, as seen from Fig. 7(b), the integrated intensity of TPFMM defined in Eq. (7) is slightly larger than that of TPM while the integrated intensity defines in Eq. (8) smaller than that of TPM. This is because of the negative sidelobes in the focal plane. However, with the increase of the zone numbers, the sidelobes become smaller and have less contribution to the integrated intensity. That is why the integrated intensity at the focal plane is almost a constant when the zone number is increased to 4.
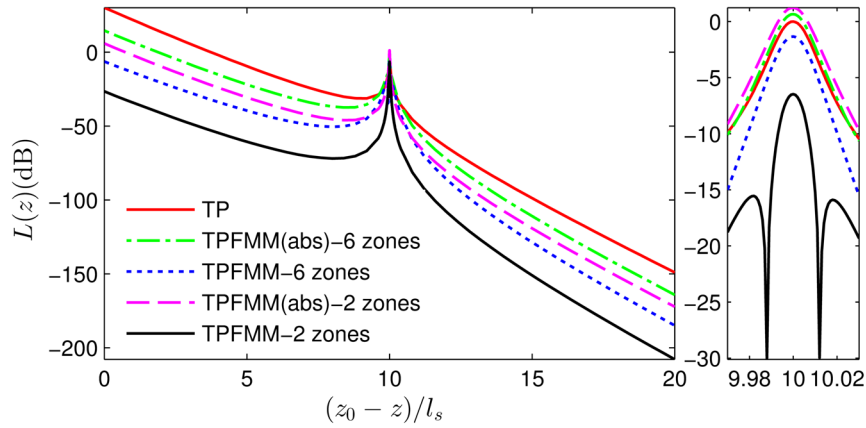
Fig. 6 The comparison of the logarithmically integrated intensity $L(z)$ for two-zone and six-zone sinusoidal filters with the imaging depth $z_0 = 1$ mm and $l_s = 100$ μm. The inset on the right is the zoom-in figure near the focal plane of the sample. TPM case is also included and the water immersion objective with NA $= 1.0$ is used.
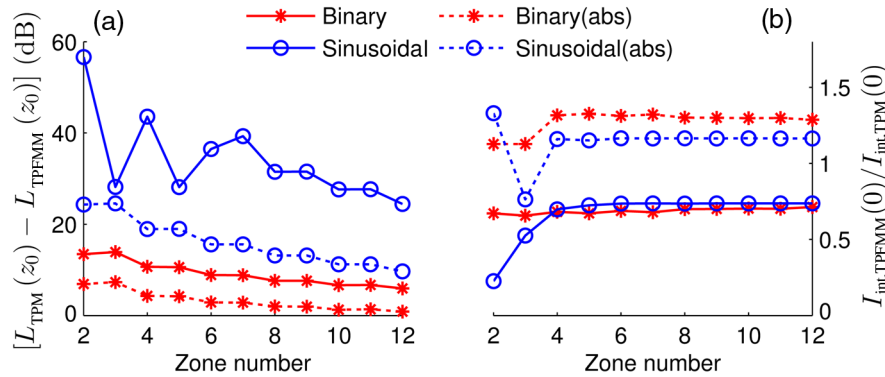

Fig. 7 (a) The difference of near-surface out-of-focus ballistic excitation between TPM and TPFMM. (b) The ratio of focal plane integrated intensity of TPFMM to that of TPM with various filters when the same illumination intensity is given. A water immersion objective lens with NA $= 1.0$ is used and imaging depth is $z_0 = 1.0$ mm.

4.4 Signal-to-Background Ratio

A more practical parameter for the deep-tissue imaging is the signal-to-background ratio, which can be defined as

$$\text{SBR} = \frac{S}{B} = \frac{\int_{V_0} I_{\text{EX}}(x, y, z) \mathrm{d}V}{\int_V I_{\text{EX}}(x, y, z) \mathrm{d}V - \int_{V_0} I_{\text{EX}}(x, y, z) \mathrm{d}V}, \quad (10)$$

where S is the focus signal and B is the out-of-focus background. Here V_0 is the focal volume and V is the full object space in the sample. Figure 8 shows the SBR of TPM and TPFMM as a function of imaging depth z_0 using sinusoidal phase filters with different zones. It can be found that when the focal depth increases to $3l_s$, the SBR of TPM begins to decay. This is because the out-of-focus fluorescence generated by scattered excitation becomes dominating. In contrast, the SBR of TPFMM using sinusoidal phase filters keep almost constant until the focal depth is about $6l_s$, where the background fluorescence mainly comes from the out-of-focus fluorescence generation near the top of the sample. When the focal depth is larger than $6l_s$, the more zones of the sinusoidal filters, the worse SBR of the TPFMM. TPFMM with sinusoidal phase filters exhibits strong potential to achieve high imaging penetration depth in the thick biological sample.

5 Discussions

The stripe-shaped phase filters are employed in TPFMM due to the ease of fabrication and alignment. It is found that the commonly used stripe-shaped binary phase filters are not a good
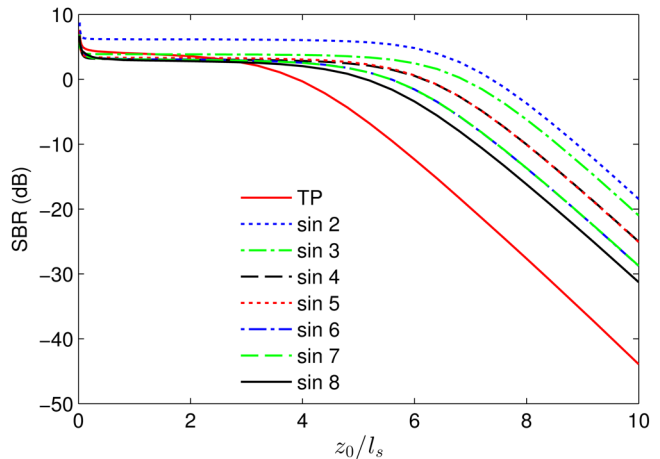

Fig. 8 The SBR of TP and TPFMM with sinusoidal filter using the definition of Eq. (8).

candidate for TPFMM. We have proposed and examined the performance of TPFMM with the proposed stripe-shaped sinusoidal phase filters, which includes the PSF, resolution, modulation depth, background suppression, and SBR. These observations have the following consequences from the practical point of view.

First, the resolution of TPFMM is almost same as TPM although the PSF of TPFMM is a subtraction of a TPM image using an inhomogeneous phase filter from another image using a homogeneous phase filter. Specifically, the TPFMM can achieve about 0.3-μm lateral resolution and 1.1-μm longitudinal resolution, when the water immersion objective with NA = 1.0 is used.

Second, there is a tradeoff between the background suppression and modulation depth when the zone number of phase filter is chosen. It is known that the better background suppression of out-of-focus ballistic excitation can be achieved with a small zone number. However, the fewer zones of the filter, the smaller the modulation depth of TPFMM and thus the lower efficiency of the FMM signal generation and signal-to-noise ratio. As an example, the modulation depth of TPFMM with a two-zone phase filter is only 0.14 although its ability of background suppression is the best. The modulation depth is so small that it is challenging to achieve a decent signal-to-noise ratio, especially in deep-tissue imaging experiments.

Based on the above analysis, the optimal phase filter should be the one that can improve background rejection with a reasonably high signal level (modulation depth). For TPFMM with a six-zone sinusoidal phase filter, the out-of-focus ballistic excitation is about 36 dB lower than TPM and the modulation depth of about 0.41 is reasonably high. The SBR of TPFMM with the same phase filter is about 15 dB better than TPM when the focal depth ranges from 5 to 10 l_s (SMFP) as shown in Fig. 8.

6 Conclusions

In summary, a stripe-shaped filter with a sinusoidal phase distribution is proposed for the STPM in TPFMM. Using the vectorial diffraction theory, we have theoretically demonstrated that TPFMM using this filter can suppress the out-of-focus ballistic excitation contribution to the background compared to the filter with sharp phase transitions. But there is a tradeoff between the background suppression and modulation depth. It is found that TPFMM using a six-zone filter can achieve the out-of-focus ballistic excitation background 36 dB lower than TPM with a reasonably high modulation depth of 0.41 and the comparable resolution as TPM. In addition, its SBR is about 15 dB better than TPM when the focal depth is from 5 to 10 l_s (SMFP). Therefore, combined with the focal modulation technique, TPFMM using a sinusoidal phase filter is expected to achieve significantly improved imaging depth. Such a theoretical study provides valuable guidance for the future experimental setup.

Disclosures

No conflicts of interest, financial or otherwise, are declared by the authors.

Acknowledgments

References

1. N. Chen, S. Rehman, and C. J. R. Sheppard, "Advanced optical microscopy methods for in vivo imaging of sub-cellular structures in thick biological tissues," *J. Innovative Opt. Health Sci.* **7**(5), 1440001 (2014).
2. A. Diaspro, *Confocal and Two-Photon Microscopy: Foundations, Applications and Advances*, Wiley, New York (2001).
3. J. G. Fujimoto et al., "Optical biopsy and imaging using optical coherence tomography," *Nat. Med.* **1**(9), 970–972 (1995).
4. P. Zhang et al., "Imaging single chiral nanoparticles in turbid media using circular-polarization optical coherence microscopy," *Sci. Rep.* **4**, 4979 (2014).
5. D. A. Dombeck et al., "Functional imaging of hippocampal place cells at cellular resolution during virtual navigation," *Nat. Neurosci.* **13**(11), 1433–1440 (2010).
6. N. Olivier et al., "Cell lineage reconstruction of early zebrafish embryos using label-free nonlinear microscopy," *Science* **329**(5994), 967–971 (2010).
7. P. Theer, M. T. Hasan, and W. Denk, "Two-photon imaging to a depth of 1000 μm in living brains by use of a Ti: Al$_2$O$_3$ regenerative amplifier," *Opt. Lett.* **28**(12), 1022–1024 (2003).
8. D. Kobat et al., "Deep tissue multiphoton microscopy using longer wavelength excitation," *Opt. Express* **17**(16), 13354–13364 (2009).
9. J. Ying, F. Liu, and R. R. Alfano, "Spatial distribution of two-photon-excited fluorescence in scattering media," *Appl. Opt.* **38**(1), 224–229 (1999).
10. A. Leray, K. Lillis, and J. Mertz, "Enhanced background rejection in thick tissue with differential-aberration two-photon microscopy," *Biophys. J.* **94**(4), 1449–1458 (2008).
11. A. Leray and J. Mertz, "Rejection of two-photon fluorescence background in thick tissue by differential aberration imaging," *Opt. Express* **14**(22), 10565–10573 (2006).
12. G. Zhu et al., "Simultaneous spatial and temporal focusing of femtosecond pulses," *Opt. Express* **13**(6), 2153–2159 (2005).
13. W. Song, J. Lee, and H.-S. Kwon, "Enhancement of imaging depth of two-photon microscopy using pinholes: analytical simulation and experiments," *Opt. Express* **20**(18), 20605–20622 (2012).
14. K. Isobe et al., "Background-free deep imaging by spatial overlap modulation nonlinear optical microscopy," *Biomed. Opt. Express* **3**(7), 1594–1608 (2012).
15. N. Chen, C.-H. Wong, and C. J. R. Sheppard, "Focal modulation microscopy," *Opt. Express* **16**(23), 18764–18769 (2008).
16. S. Pant et al., "Line-scan focal modulation microscopy," *J. Biomed. Opt.* **22**, 050502 (2017).
17. S. Pant et al., "Augmented line-scan focal modulation microscopy for multi-dimensional imaging of zebrafish heart in vivo," *Biomed. Opt. Express* **8**, 5698–5707 (2017).
18. S. P. Chong et al., "High-speed focal modulation microscopy using acousto-optical modulators," *Biomed. Opt. Express* **1**(3), 1026–1033 (2010).
19. N. Chen and G. J. Gao, "Multi-contrast focal modulation microscopy for in vivo imaging of thick biological tissues," *Opt. Express* **20**(11), 12166–12170 (2012).
20. K. Si et al., "Two-photon focal modulation microscopy in turbid media," *Appl. Phys. Lett.* **99**(23), 233702 (2011).
21. E. Wolf, "Electromagnetic diffraction in optical systems. I. An integral representation of the image field," *Proc. R. Soc. London Ser. A* **253**(1274), 349–357 (1959).
22. R. Chen et al., "A complete and computationally efficient numerical model of aplanatic solid immersion lens scanning microscope," *Opt. Express* **21**(12), 14316–14330 (2013).
23. C. J. R. Sheppard and M. Gu, "Image formation in two-photon fluorescence microscopy," *Optik* **86**(3), 104–106 (1990).
24. M. Born and E. Wolf, *Principles of Optics*, Elsevier Science, Amsterdam (2013).
25. M. Gu, *Advanced Optical Imaging Theory*, Springer, Berlin (2000).

Biographies for the authors are not available.